Room-temperature photon avalanche upconversion in Tm^{3+}:Y_2O_3 crystals

I. R. Martín
Departamento de Física Fundamental y Experimental, Universidad de La Laguna, 38206 La Laguna, Tenerife, Spain

C. Goutaudier, S. Guy, Y. Guyot, G. Boulon, M.-T. Cohen-Adad, and M.-F. Joubert
Laboratoire de Physico-Chimie des Matériaux Luminescents, UMR No. 5 620 CNRS, Université Lyon 1, 43 boulevard 11 Novembre 1918, 69622 Villeurbanne Cedex, France
(Received 29 April 1999)

Photon avalanche red to blue upconversion has been observed at room temperature in 2% Tm^{3+}:Y_2O_3 and 3% Tm^{3+}:Y_2O_3 crystal fibers under excitation at 628.7 nm. The dynamics and power dependence of upconversion emission corresponding to the $^1G_4 \rightarrow {}^3H_6$ transition have been investigated using the mean field approximation. [S0163-1829(99)12733-4]

I. INTRODUCTION

The photon avalanche effect is a phenomenon that has been observed in a lot of rare earth doped materials (see Ref. 1 for a review). For this upconversion process, the pump photon energy is only resonant between a metastable state and a higher level of the active ions. The main characteristic of such a process is an excitation power threshold which corresponds to a sudden absorption of the pump photons and, therefore, to a sudden increase of the upconverted fluorescence. At the same time, there is a slowing down and a change of the rise shapes of the transient signals. This upconversion mechanism is very spectacular in several Tm^{3+}-doped oxides or fluorides: after pumping in the red range, very intense blue fluorescence around 480 and/or 450 nm (depending on the host) occurs with all the characteristics of the photon avalanche effect. Moreover, in most Tm^{3+}-doped materials, such a photon avalanche effect occurs from cryogenic temperature up to room temperature, which is of great interest in view of upconversion laser application.

This paper is devoted to the case of a Tm^{3+}-doped yttria single crystal which is one of the best host laser materials due to adapted physical and chemical properties for laser operation. First, we will present a brief summary of the theoretical photon avalanche model and the method we choose to evaluate the spectroscopic parameters involved in the rate equation system. Then we will describe the material and the experimental equipment. Finally, the experimental results will be presented and discussed and it will be concluded that photon avalanche red to blue upconversion occurs in 2 and 3 at. % Tm^{3+}-doped Y_2O_3 single crystals.

II. THEORETICAL MODEL

A lot of papers are providing general and theoretical approaches to the photon avalanche.[2–7] More recently, by comparing this nonlinear upconversion process to a second order phase transition and using the general Landau theory, the fundamental physics associated with such upconversion has been elucidated.[8] The first part of this section gives the rate equation system used for photon avalanche especially in the case of red to blue upconversion in Tm^{3+}-doped compounds. Then the following parts describe the method we choose to evaluate the cross relaxation energy transfer rates and the saturation rate of the metastable state.

A. Photon avalanche rate equation system

The photon avalanche process leading to the strong blue emission ($^1G_4 \rightarrow {}^3H_6$) of Tm^{3+} ions after red excitation resonant with the $^3F_4 \rightarrow {}^1G_4$ transition has been studied in different materials. The microscopic description of this process is schematized in Fig. 1. As all ions are initially in the ground state 1 (no thermal population of level 2), the effect of the pump is minimal. If one ion is promoted to the metastable state 2, whatever the mechanism by which this state is populated, it may be further excited to level 4 by absorption of the pump photon. Then, due to high concentration, this ion can interact with two neighbors: a first cross relaxation energy transfer promotes one neighbor ion into the $^3F_4$ level, the initial excited ion decaying to the $^3H_4$ state 3 from which another cross relaxation energy transfer results in two other

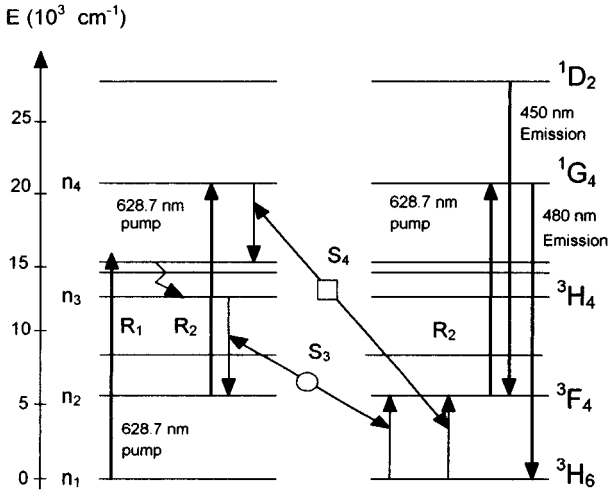

FIG. 1. Schematic energy level diagram of Tm^{3+}:Y_2O_3 illustrating the photon avalanche process.

ions in the metastable level. Now, three ions are available for further absorption of the pump light. Next, by the same feeding process, nine ions are excited to the metastable state and so on. A simple and clear interpretation of this process may be done using the following rate equation system:

$$dn_4/dt = R_2 n_2 - W_4 n_4 - s_4 n_1 n_4, \tag{1}$$

$$dn_3/dt = R_1 n_1 - (W_3 + W_3^{NR}) n_3 + b_{43} W_4 n_4 + s_4 n_1 n_4 - s_3 n_3 n_1 + Q_{23} n_2^2, \tag{2}$$

$$dn_2/dt = -(R_2 + W_2) n_2 + b_{42} W_4 n_4 + (b_{32} W_3 + W_3^{NR}) n_3 + s_4 n_1 n_4 + 2 s_3 n_1 n_3 - (Q_{22} + 2Q_{23}) n_2^2, \tag{3}$$

$$n_1 + n_2 + n_3 + n_4 = 1. \tag{4}$$

It is assumed that the first step promoting at least one ion in $^3F_4$ occurs via the nonresonant phonon sideband ground state absorption above the $^3F_2$ level followed by fast nonradiative decay to $^3H_4$. Then, different desexcitation channels can feed up the metastable level. So, Eqs. (1)–(4) involve the ground and excited state pumping rates R_1 and R_2, the single ion radiative relaxation rates W_i of level i, and the branching ratios b_{ij} from level i to level j. These W_i and b_{ij} parameters can be calculated using the well known Judd-Ofelt theory.[9] The multiphonon relaxation rate from level 3, W_3^{NR}, is the only one which cannot be neglected. Its value is obtained by comparison of the calculated radiative relaxation rate W_3 and of the $^3H_4$ fluorescence lifetime measured in a very low concentrated crystal. The cross relaxation energy transfers are described by the parameters s_3 and s_4 which include nonlinear terms in the rate equations these parameters are evaluated experimentally using the methods described in Sec. II B. At high excitation power, the metastable state population is high enough to be saturated and this is described by the parameters Q_{ij}. Q_{23} corresponds to the following upconversion energy transfer:

$$^3F_4 + {}^3F_4 \rightarrow {}^3H_6 + {}^3H_4 \tag{5}$$

which is the inverse process of the cross relaxation s_3. Q_{22} describes the following upconversion process:

$$^3F_4 + {}^3F_4 \rightarrow {}^3H_6 + {}^3H_5 \tag{6}$$

followed by rapid nonradiative decay from $^3H_5$ to $^3F_4$.

B. Cross relaxation energy transfer rates

If τ_0 is the single ion lifetime of level i and η_i is the quantum yield of the cross relaxation mechanism from this level, then

$$\eta_i = \frac{s_i}{\tau_0^{-1} + s_i} = 1 - \frac{\int_0^\infty I(t)dt}{\tau_0 I(0)}, \tag{7}$$

where $I(t)$ is the fluorescence intensity emitted from level i. So

$$s_i = \frac{\eta_i}{\tau_0(1-\eta_i)}. \tag{8}$$

This is the way we choose to evaluate experimentally the cross relaxation energy transfer rates from the levels $^3H_4$ and $^1G_4$, described by the parameters s_3 and s_4 respectively. This method has the big advantage that the estimation of η_i is directly done from the experimental decay curve of the emitting level.

C. Upconversion rate from $^3F_4$

The upconversion rate from $^3F_4$ can be obtained by analysing the $^3F_4$ fluorescence decay versus the initial population of this level. This procedure has been used previously to get the upconversion rates in Nd^{3+}-doped YAG crystals.[10] The rate equation that describes the $^3F_4$ population of Tm^{3+} ions, after direct pulsed excitation into this level, is given by

$$\frac{dn_2}{dt} - W_2 n_2 - Q n_2^2, \tag{9}$$

where $Q = Q_{22} + 2*Q_{23}$. The solution to this equation is

$$n_2(t) = \frac{n_2(0)\exp(-W_2 t)}{1 + Q n_2(0)[1 - \exp(-W_2 t)]}. \tag{10}$$

At low doping concentration and weak excitation powers, the decay curves have an exponential shape. However, the upconversion processes produce an increasing nonexponentiality with the excitation power. The overall lifetime of the decay curves is defined by

$$\langle \tau \rangle = \frac{\int I(t)dt}{I(0)}, \tag{11}$$

where $I(t)$ is the fluorescence intensity (corresponding to the transition $^3F_4 \rightarrow {}^3H_6$) which is proportional to $n_2(t)$. In order to compare these experimental results with the theoretical expressions, the profile of the excitation beam must be taken into account. In a Gaussian profile excitation, the overall lifetime can be obtained as

$$\langle \tau \rangle = \frac{\int \left(\int n_2(t,r) 2\pi r dr \right) dt}{\int n_2(0,r) 2\pi r dr}. \tag{12}$$

So, the procedure for evaluating experimentally the upconversion rate consists first to get the W_2 value at weak excitation (by fitting the $^3F_4 \rightarrow {}^3H_6$ decay curve to exponential). Then, by increasing the excitation energy, the experimental overall lifetimes are measured and fitted to the Eq. (12).

III. MATERIAL

Yttria is a very attractive optical material for several reasons: it is a refractory oxide with a melting point of about 2450 °C, a very high thermal conductivity of 33 $W\,m^{-1}\,K^{-1}$ and a density of 5.03 $g\,cm^{-3}$. In addition, this crystal has the

cubic body centered structure with the space group $Ia3(T_h^7)$, then it is optically isotropic with a refractive index of 1.91. Another interesting property allowing radiative transitions between electronic levels is that the dominant phonon energy in this material[11] is 380 cm^{-1} which is one of the smallest phonon cutoff among oxides. In the unit cell, there are eight cation centrosymmetric sites having a point symmetry of $C_{3i}(S_6)$ and 24 cation non-centro-symmetric sites having a point symmetry of C_2. These two types of sites can be occupied with approximately equal probability, however, investigations of optical absorption and fluorescence spectra of trivalent rare earth ions in yttria established that the optical transitions mostly occur within the ions at the C_2 sites for which forced electric dipole transitions are allowed.[12–15] A precise determination of Tm^{3+} Stark-level energies in yttria was done up to the $^1D_2$ manifold[14] and Judd-Ofelt calculation was performed to get the radiative lifetimes and branching ratios.[16]

Tm^{3+}-doped Y_2O_3 single crystals used in this work were grown in the form of fibers by the Laser Heated Pedestal Growth technique described previously.[16] They were doped with 0.5, 1, 2, 3, or 5 at. % of Tm^{3+} with respect to Y^{3+}.

IV. EXPERIMENTAL

All the spectroscopic measurements were done at room temperature and using the experimental equipment described in this section. The cross relaxation rates from $^1G_4$ as well as from $^3H_4$ were measured by analyzing the $^1G_4$ and $^3H_4$ fluorescence decays respectively versus Tm^{3+} concentration in each sample. Selective excitation in the $^1G_4$ state was performed using an excimer laser (pulse length: 10 ns, variable repetition rate and energy per pulse up to 50 mJ at 308 nm) followed by a one-amplifier-stage dye laser (pulse length: 10 ns and line width: 0.1 cm^{-1}) containing a Coumarin 480 solution. Selective excitation in the $^3F_2$ state was performed using a frequency doubled Nd:YAG laser (pulse length: 10 ns, repetition rate: 10 Hz, and energy per pulse up to 300 mJ at 532 nm) followed by a three-amplifier-stage dye laser (pulse length: 10 ns and line width: 0.1 cm^{-1}) containing a DCM solution. The sample fluorescence was analyzed by a 1 m Hilger and Watts monochromator with a dispersion of 0.8 nm/mm and detected by a RCA GaAs photomultiplier tube. The signal was processed by an Ortec photon counting system. The fluorescence decay time measurements were realized using a Canberra 35+ multichannel analyzer with a maximum resolution of 200 ns per channel.

The saturation rate of the $^3F_4$ metastable state was measured by analyzing the $^3F_4$ fluorescence decay versus the excitation density. Selective excitation in $^3F_4$ was performed with the frequency doubled Nd:YAG pumped dye laser containing pyridine 1 solution and followed by a Raman cell. The excitation intensity was varied using neutral density filters and the Gaussian beam was focused in the sample with a 500 mm lens. The waist spot size on the sample (defined as the $1/e^2$ radius of the intensity) was shown to be $100 \times 100\,\mu m^2$. The emission was analyzed with a $\frac{1}{4}$-m Jobin-Yvon monochromator with a dispersion of 6 nm/mm followed by an AsIn detector. The signal was acquired by a Lecroy 9410 digital oscilloscope controlled by a personal computer.

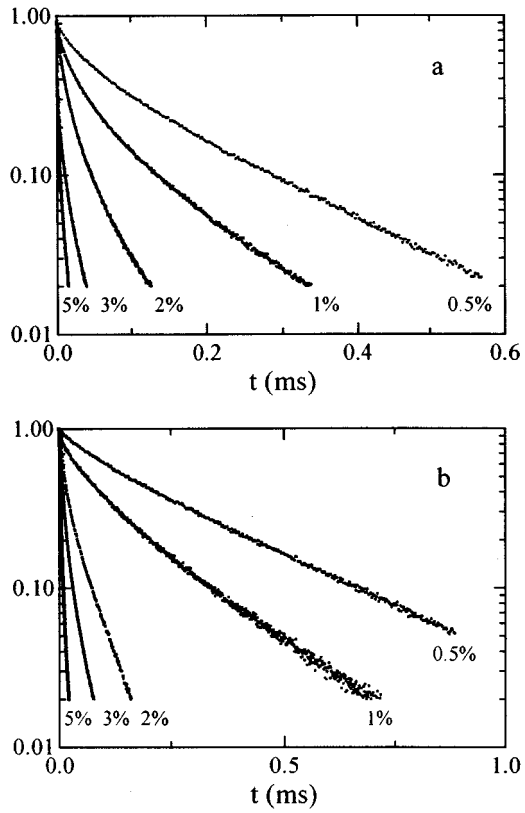

FIG. 2. (a) $^1G_4 \rightarrow {}^3F_4$ fluorescence decay recorded after excitation at 476 nm in Tm^{3+}:Y_2O_3 crystals versus Tm^{3+} concentration. (b) $^3H_4 \rightarrow {}^3H_6$ fluorescence decay recorded after excitation at 680 nm in Tm^{3+}:Y_2O_3 crystals versus Tm^{3+} concentration.

For photon avalanche pumped unconverted fluorescence, laser excitation was achieved by a continuous wave Ar^+ laser pumped ring dye laser with Kiton red solution. The laser beam was chopped and focused on the sample with a 50 mm lens. The waist spot size in the sample was shown to be $15 \times 15\,\mu m^2$. The anti-Stokes fluorescence was collected at a right angle to the laser beam direction and was analyzed by a $\frac{1}{4}$-m Jarrel-Ash monochromator followed by an EMI 9789QB photomultiplier. The signal was acquired by a Lecroy 9410 digital oscilloscope for dynamics study or by an digital analogic card for spectral study. All this experimental setup was controlled by a personal computer.

V. EXPERIMENTAL RESULTS AND DISCUSSION

A. Cross relaxation energy transfer rates

After selective excitation in $^1G_4$ (476 nm) and in $^3F_2$ (680 nm), we recorded the $^1G_4 \rightarrow {}^3F_4$ and $^3H_4 \rightarrow {}^3H_6$ fluorescence decays respectively versus Tm^{3+} concentration. They are presented in Fig. 2. Then, we deduced from each decay the cross relaxation quantum yield η_i for these two emitting levels as well as the cross relaxation rates. The results are given in Table I. It is clear, as expected, that the efficiency of the cross relaxation energy transfers increases dramatically with Tm^{3+} concentration. In the 2 at. % doped crystals they are already the dominant processes responsible for the $^1G_4$ and $^3H_4$ relaxation.

TABLE I. Spectroscopic parameters of the Tm^{3+}-doped Y_2O_3 at room temperature.

W_3 (ms^{-1})	1.362	calculated radiative relaxation rate (Ref. 15)
W_3^{exp} (ms^{-1})	2.439	measured in very low concentrated crystal (Ref. 13)
W_3^{NR} (ms^{-1})	1.077	$W_3^{exp}-W_3$
W_4 (ms^{-1})	4.167	measured in very low concentrated crystal (Ref. 13)
b_{ij}	$b_{32}=0.12$	Ref. 15
	$b_{42}=0.35$	Ref. 15
	$b_{43}=0.13$	Ref. 15

Concentration:	0.5%	1%	2%	3%	5%
W_2 (ms^{-1})	0.258	0.263	0.267	0.274	0.308
η_3	0.350	0.672	0.912	0.971	0.991
η_4	0.485	0.747	0.915	0.982	0.996
s_3 (ms^{-1})	1.4	5.0	25.3	81.7	268
s_4 (ms^{-1})	3.9	12.3	44.9	227	1038
Q (ms^{-1})			0.31	0.55	0.92

B. Upconversion rate from $^3F_4$

Under pulsed laser excitation into the $^3F_4$ level (1631.8 nm) in different concentrated samples infrared luminescence at 800 nm corresponding to the $^3H_4 \rightarrow {}^3H_6$ transition can be detected. This process can be explained according to the channel given by (5). Using the method given in Sec. II C, we were able to estimate the rate of the upconversion from $^3F_4$. Under weak excitation densities, the $^3F_4 \rightarrow {}^3H_6$ decay curves have an exponential shape. However, the upconversion processes produce an increasing nonexponentiality with the excitation power. This effect has been observed in the decay curves obtained in the 2, 3, and 5 at. % Tm^{3+}-doped Y_2O_3. The shortened overall lifetime of the $^3F_4$ level obtained with samples doped with these three concentrations is shown in Fig. 3. As can be seen in this figure, a significant decrease of this lifetime is observed when the excitation power is increased. Good fits to Eq. (10) are found for the different doped samples leading to a value of the upconversion rate equal to 0.31, 0.55, and 0.92 ms^{-1} for the 2, 3, and 5 at. % Tm^{3+}-doped Y_2O_3, respectively. These upconversion rate values reflect the effect of the two processes described by (5) and (6). We know that Q_{23} is efficient because we observed the $^3H_4 \rightarrow {}^3H_6$ emission after excitation into the $^3F_4$. But we have no way to estimate the relative efficiencies of Q_{22} and Q_{23}. Nevertheless, regarding the energy gap differences for these two processes it appears that $\Delta E = 2972\,cm^{-1}$ (8 phonons) for the former and $\Delta E = 1326\,cm^{-1}$ (3–4 phonons) for the later suggesting that Q_{22} is probably much lower than Q_{23}.

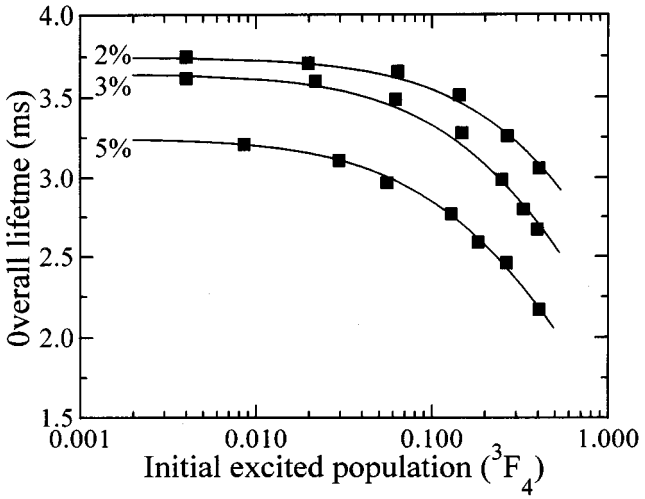

FIG. 3. Variation of the overall lifetime with the initial excited $^3F_4$ population for different doped samples. The solid lines show the theoretical lifetime obtained from the rate equation taking into account the gaussian beam profile.

C. Red to blue photon avalanche upconversion

We observed red to blue upconversion emission in Tm^{3+}-doped Y_2O_3 crystals by exciting in the 618–657 nm range with the cw dye laser. As an example, the upconversion spectrum shown in Fig. 4 was recorded under excitation at 654.1 nm with the 2 at. % Tm^{3+}-doped Y_2O_3 sample. Emission peaks centered around 450 and 480 nm are attributed to the transitions $^1D_2 \rightarrow {}^3F_4$ and $^1G_4 \rightarrow {}^3H_6$. Similar spectra have been obtained in samples with different concentrations of Tm^{3+}. The excitation spectrum obtained detecting

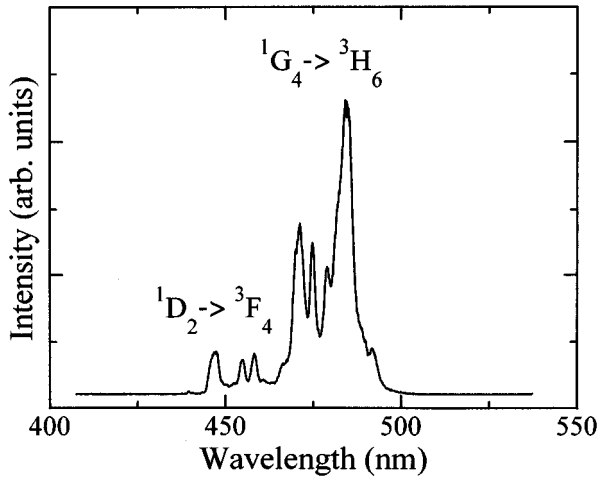

FIG. 4. Upconversion emission spectrum obtained under excitation at 654.1 nm in Y_2O_3: 2 at. % Tm^{3+}.

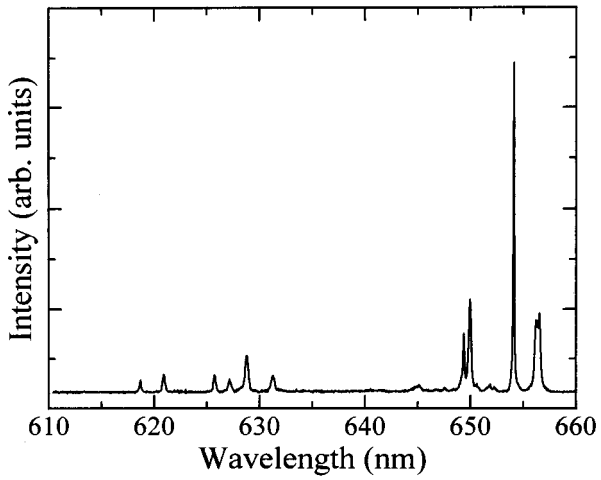

FIG. 5. Excitation spectrum obtained detecting at 487 nm in Y_2O_3: 2 at. % Tm^{3+}.

at 487 nm is presented in Fig. 5 always with the 2 at. % Tm^{3+}-doped Y_2O_3 sample. Using the positions of the energy levels given in Ref. 13, all the peaks observed in this figure can be attributed to transitions between the Stark components of the $^3F_4$ and the $^1G_4$ manifolds and this spectrum is in good agreement with the $^3F_4 \rightarrow {}^1G_4$ excited state excitation spectrum presented recently.[17] In order to investigate the upconversion mechanism of the blue upconversion emission, we recorded the excitation power dependence of its intensity. When the excitation is carried out at 654.1 nm the blue upconversion emission presents a quadratic dependence with the excitation intensity while, when we used an excitation wavelength of 628.7 nm, a soft sudden increase of the upconverted fluorescence is observed nearly to $P_{exc}=51$ mW. This result is presented in Fig. 6 in which are also included the values for the time of establishment T_e of the blue upconverted fluorescence, defined as the time necessary to reach 95% of the blue stationary intensity. In Fig. 7 are presented the experimental rise curves of this blue emission ob-

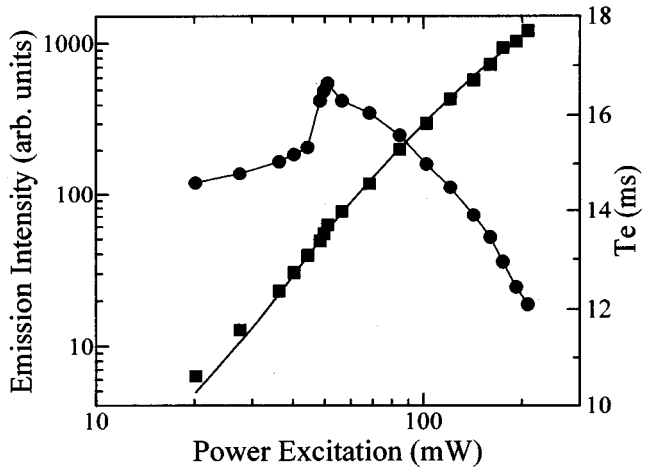

FIG. 6. Upconversion emission stationary intensity (■) and time of establishment (●–●) obtained in Y_2O_3: 2 at. % Tm^{3+} after excitation at 628.7 nm and detecting at 487 nm. The solid line is the fit to the expression indicated in the text.

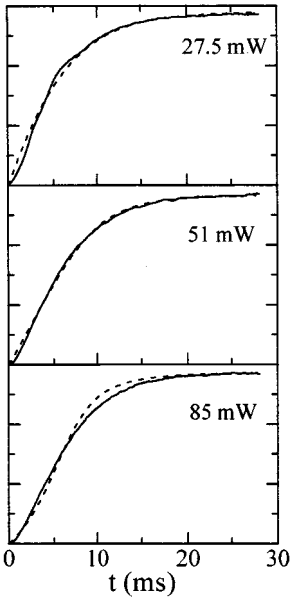

FIG. 7. Experimental rise curves (solid line) of the blue fluorescence at 487 nm for different pump intensities at 628.7 nm obtained in Y_2O_3: 2 at. % Tm^{3+}. The dashed lines correspond to the fits to the expression indicated in the text.

tained for different pump intensities at 628.7 nm always in the Y_2O_3: 2 at. % Tm^{3+}. All these experimental results (changes of the rise shapes with, at a given threshold value, a critical slowing down and a sudden increase of the stationary intensity) are characteristic of a photon avalanche excitation process. In the 3 at. % Tm^{3+}-doped Y_2O_3 sample, we also observed an avalanche effect by exciting at 628.7 nm with an experimental excitation power threshold of 74 mW, which is a little bit higher than in the 2 at. %-doped sample. Moreover, the values obtained for the critical slowing down, defined as the ratio of T_e over the metastable state lifetime τ_2, are 4.4 and 3.6 for the 2 and 3 at. % doped samples, respectively. An avalanchelike behavior has been reported previously in 2 at. % Tm^{3+}-doped Y_2O_3 crystal fibers at temperature of 12 K (Ref. 18) but the authors did not observed a sharp threshold behavior because they used an excitation wavelength of 653.7 nm. As this value is in the $^3H_4 \rightarrow {}^1D_2$ spectral range[16] and also close to a $^3H_6 \rightarrow {}^3F_2$ resonance, step by step absorption process is efficient and the avalanche effect is not so evident to see than under lower excitation wavelength excitation where only $^3F_4 \rightarrow {}^1G_4$ resonance exists.

The transient curves for the photon avalanche upconverted blue emission in Y_2O_3: 2 at. % Tm^{3+} as well as the curve relative to the excitation power dependence of the stationary blue intensity have been calculated using the rate equation system (1)–(4) and the spectroscopic parameters determined in Sec. V A and V B and taking into account the Gaussian profile of the laser beam.[8] In the calculation all the spectroscopic parameters are fixed except R_1 and R_2. The best fits are obtained assuming $Q_{22}=0$ and the results are shown in Figs. 6 and 7. From these fits, we obtained the cross sections $\sigma_1=R_1/I=1.2\times10^{-21}\,\mathrm{cm}^2$ and $\sigma_2=R_2/I=4.4\times10^{-21}\,\mathrm{cm}^2$. The low value obtained for the ratio

σ_2/σ_1 is indicative of the low avalanche effect observed in this material compared to that observed in Tm^3:YAG for example.[8]

VI. CONCLUSION

We have observed blue emission when pumping in the 615–660 nm range at room temperature in Tm^{3+}:Y_2O_3 crystals. For an excitation wavelength of 628.7 nm, the photon avalanche effect is demonstrated. Nevertheless, it gives rise to lower blue emission intensity than when the excitation wavelength is around 655 nm for which $^3F_4 \rightarrow {}^1G_4$, $^3H_4 \rightarrow {}^1D_2$ as well as $^3H_6 \rightarrow {}^3F_2$ resonances exists.

ACKNOWLEDGMENT

This work has been partially supported by ''Gobierno Autónomo de Canarias.''

[1] M.-F. Joubert, Opt. Mater. **11**, 181 (1999).
[2] W. E. Case, M. E. Koch, and A. W. Kueny, J. Lumin. **45**, 351 (1990).
[3] M.-F. Joubert, S. Guy, and B. Jacquier, Phys. Rev. B **48**, 10 031 (1993).
[4] M.-F. Joubert, S. Guy, B. Jacquier, and C. Linarés, Opt. Mater. **4**, 43 (1994).
[5] A. Brenier, L. C. Courrol, C. Pédrini, C. Madej, and G. Boulon, Opt. Mater. **3**, 25 (1994).
[6] M. Bouffard, J. P. Jouart, and G. Mary, J. Phys. (France) **6**, 691 (1996).
[7] F. Auzel and Y. Chen, J. Lumin. **65**, 45 (1995).
[8] S. Guy, M.-F. Joubert, and B. Jacquier, Phys. Rev. B **55**, 8240 (1997).
[9] B. R. Judd, Phys. Rev. **127**, 750 (1962); G. S. Ofelt, J. Chem. Phys. **37**, 511 (1962).
[10] S. Guy, C. L. Bonner, D. P. Shepherd, D. C. Hanna, A. C. Tropper, and B. Ferrand, IEEE J. Quantum Electron. **34**, 900 (1998).
[11] G. Schaack and J. A. Koningstein, J. Opt. Soc. Am. **60**, 1110 (1970).
[12] J. B. Gruber, W. F. Krupke, and J. M. Poindexter, J. Chem. Phys. **41**, 3363 (1964).
[13] W. F. Krupke, Phys. Rev. **145**, 325 (1966).
[14] M. J. Weber, Phys. Rev. **171**, 283 (1968).
[15] R. P. Leavitt, J. B. Gruber, N. C. Chang, and C. A. Morrison, J. Chem. Phys. **76**, 4775 (1982).
[16] F. S. Ermeneux, C. Goutaudier, R. Moncorgé, M.-T. Cohen-Adad, M. Bettinelli, and E. Cavalli, Opt. Mater. **8**, 83 (1997).
[17] N. Garnier, R. Moncorgé, H. Manaa, E. Descroix, P. Laporte, and Y. Guyot, J. Appl. Phys. **79**, 4323 (1996).
[18] J. M. Dyson, S. M. Jaffe, H. Eilers, M. L. Jones, W. M. Dennis, and W. M. Yen, J. Lumin. **60&61**, 668 (1994).